

A Molecularly Imprinted Polymer@PtNPs/MoS₂-Based Electrochemical Platform for Sensing Glycated Albumin Concentration on the Screen-Printed Electrode (SPE)

Sunil Kumar Mahobiya¹ , Sapna Balayan¹ , Nidhi Chauhan¹ , Naresh Kumar Kuchhal² , Saikh Safiul Islam³ , Utkarsh Jain^{1,*} 

¹ Amity Institute of Nanotechnology (AINT), Amity University Uttar Pradesh (AUUP), Sector -125, Noida- 201313, Uttar Pradesh, India; ksunil912@gmail.com (S.K.); sbalayan@amity.edu (S.B.); nchauhan1@amity.edu (N.C.); ujain@amity.edu (U.J.);

² Bio Diagnostic Laboratory, Rohini, Delhi-110085, India; nkkuchhal@gmail.com (N.K.K.);

³ Centre for Nanoscience & Nanotechnology, Jamia Millia Islamia, Jamia Nagar, New Delhi-110025, India; sislam@jmi.ac.in (S.S.I.);

* Correspondence: ujain@amity.edu, karshjain@gmail.com (U.J.);

Scopus Author ID 56534847500

Received: 5.06.2022; Accepted: 10.07.2022; Published: 17.09.2022

Abstract: A majority of the population is affected by diabetes worldwide. The delay in detection leads to serious conditions such as cardiovascular disease, neuropathy, and others. To avoid severe consequences, it needs to be detected at the early stages. Various methods and techniques have already been introduced commercially to detect diabetes. But still, there are various limitations to these traditional methods (ion-exchange chromatography, high-performance liquid chromatography (HPLC), thiobarbituric acid (TBA) assay, boronate affinity chromatography) such as they require more time for operation; also, they are expensive and need expertise for operation. These limitations can be overcome with the application of biosensors integrated with nanomaterials and imprinting techniques. This presented study describes the development of an electrochemical biosensing platform for determining the concentration of glycated albumin. The biosensor was developed using the molecularly imprinting technique to enhance the specificity, stability, and selectivity. Further, to enhance the electrode's conductivity, surface area, and biocompatibility, the sensing platform was modified with Molybdenum disulfide (MoS₂) nanosheets and Platinum nanoparticles (Pt NPs). Furthermore, the presented electrode was evaluated with electrochemical measurements. The biosensor exhibits a detection limit as low as 0.34 nM. Also, it operates in a dynamic concentration range from 0.34 nM to 700 μM. The actual working range was divided into lower (0.34 nM to 35 μM) and higher (200 to 700 μM).

Keywords: diabetes; nanomaterials; biosensor; electrochemical; molecularly imprinted polymer.

© 2022 by the authors. This article is an open-access article distributed under the terms and conditions of the Creative Commons Attribution (CC BY) license (<https://creativecommons.org/licenses/by/4.0/>).

1. Introduction

Diabetes mellitus is a major health issue worldwide, and it has severely affected developed countries [1-3]. A report issued in 2014 by the International Federation of Diabetes shows 382 million diabetes cases around the globe. About 300 million were recorded at higher risk of diabetes and 175 million as undiagnosed diabetics [4]. The diabetic condition in people can lead to serious complications such as cardiovascular disease, neuropathy, and retinopathy due to long-term hyperglycemia [2,5]. Therefore, the diagnosis is necessary during the early stages and taking measures to control the blood sugar within a normal range [2]. Various

published reports show that higher fluctuation in glucose levels results in macrovascular and cardiovascular diseases at the early stages. Therefore, these disorders can be prevented when detected at an early stage [2].

The available test for glucose monitoring is Glycated hemoglobin (HbA1c). It also provides information on other complications associated with a diabetic condition [6,7]. Although, in various conditions such as pregnancy, kidney-related issues, and hemoglobinopathies, the test for glycated hemoglobin is not suggested [8]. In these conditions, it is advised to measure the level of fructosamines or glycated albumin (GA) [9, 10]. GA is considered an appropriate biomarker for detecting diabetic conditions as it contains all the glycated proteins in the plasma [11]. It was first reported by Dolhofere and Weiland in 1979 that in diabetic patients level of GA is higher than measured in healthy individuals [12,13] (Healthy adults: 9-16%; Older adults: 10.23-14.79%; Children: 10.38-13.89%; Hemoglobinopathy: 14%-17%; Pregnancy: First trimesters:11.26–15.10%, Second trimesters: 10.04–13.50%, Third trimesters: 9.76–13.09%; Kidney related issues: 15.6–18.2%) [14-18]. It has been reported that the half-life of GA in the blood is 12-21 days; hence, it plays an important role in keeping track of the changes that have occurred during the glycemic condition when undergoing treatment [19-22]. Presently, GA is determined in a blood sample using traditional fructosamine tests. These tests provide most of GA signals, whereas other signals consist of glycated globulins. Several methods have already been developed for determining protein levels, such as high-performance liquid chromatography (HPLC), immunoassay, and enzyme-linked boronate-immunoassay [23]. But these methods have some constraints. They are expensive, don't provide rapid results, and require expertise for operation. These drawbacks or limitations of the traditional methods can be eliminated with the development of biosensors. The development of sensors for biomedical applications has facilitated overcoming several limitations of the conventional methods as they provide rapid results, are low cost, and are user-friendlier.

Therefore, in this presented research, an electrochemical-based biosensing platform was developed for identifying the concentration of GA in patients. Several studies have been reported for GA detection, some of which are discussed here. A study describes an electrochemical biosensor fabricated using reduced graphene oxide/gold nanoparticles (rGO/Au NPs). The biosensor is based on aptamer and anti-GA aptamer. The sensing platform was examined using various techniques. The working range of the biosensor was observed between 2-10 $\mu\text{g mL}^{-1}$ [22]. Another study describes the fabrication of a biosensor based on electrochemical and colorimetric detection of GA. A sandwich-type biosensor was fabricated using Boronic acid (BA)-agarose beads for capturing GA, and the surface was modified with urchin-like platinum nanozymes (SuPtNZs) for better sensor performance. The biosensor reported a low detection limit and higher sensitivity [24]. An aptamer-based biosensor was developed and modified with DNA for detecting glycated human serum albumin (GHSA). The sensing platform was based on graphene oxide (GO) and aptamer (Cy5- labeled G8) fluorescent quenching. The biosensor promised to monitor the level of GHSA for diabetes mellitus, and the sensor showed a detection limit of 50 $\mu\text{g mL}^{-1}$ [25]. The reported biosensors are based on enzymatic reactions that limit certain parameters such as the sensor's stability, selectivity, and storage time. The present work can facilitate overcoming these limitations.

The presented electrochemical biosensor is developed based on molecularly imprinting techniques. The molecularly imprinted polymer (MIP) for GA was synthesized and used for electrode modification. The MIP is highly specific to the predefined biomolecules and is based

on developing 3-dimensional (3-D) structures for the specific biomolecule. This technique can facilitate the improvement of the sensing platform by providing high selectivity and sensitivity [26-29]. Further, the electrode was modified with nanosheets and nanoparticles due to their exclusive properties. The advancement in 2-dimensional (2-D) materials has attracted several applications due to their unique properties, such as high stability, excellent electroactivity, low cost, and providing a large surface area. Hence, in this work, Molybdenum disulfide (MoS_2) nanosheets were incorporated; they improve the performance of a biosensor in terms of better electrical properties, increased surface area, higher electron transport, and great flexibility [30-33]. Additionally, the electrode was modified with platinum nanoparticles (Pt NPs). They are noble metal nanoparticles with various unique properties such as biocompatibility, higher conductivity, and catalytic properties [34]. The combination of MoS_2 nanosheets and Pt NPs provide a synergistic effect on the developed biosensor and improve its performance.

The fabricated biosensor exhibits a lower detection limit and rapid detection. The biosensor promises to show higher sensitivity and can be developed as a point-of-care device. Also, the sensor operates in a wide detection range.

2. Materials and Methods

The screen-printed electrode (SPE) was purchased from PalmSens Compact Electrochemical Interfaces (a company in Netherland). Azobisisobutyronitrile (AIBN, 98%), ammonium heptamolybdate tetrahydrate ($(\text{NH}_4)_6\text{Mo}_7\text{O}_{24}$), Methyl methacrylate (MMA), Ethylene glycol dimethacrylate (EGDMA), thiourea ($\text{CH}_4\text{N}_2\text{S}$), glycated human albumin, Acetonitrile (ACN), Chloroplatinic acid ($\text{H}_2\text{PtCl}_6 \cdot 6\text{H}_2\text{O}$), Trisodium citrate ($\text{Na}_3\text{C}_6\text{H}_5\text{O}_7$) were acquired from the U.S.A. based company Sigma Aldrich. The solutions were prepared in distilled water (DW).

Further, the structures on the surface of a developed platform were studied with the surface characterization technique scanning electron microscopy (SEM). Also, the reactions occurring on the modified electrode surface were recorded with electrochemical measurements on an instrument, "potentiostat SP-200 from Biologics".

2.1. Synthesis of MoS_2 nanosheets.

The MoS_2 nanosheets were synthesized by a one-step hydrothermal reaction. A mixture was prepared in 36 mL DW containing $(\text{NH}_4)_6\text{Mo}_7\text{O}_{24}$ (1.24 gm) and $\text{CH}_4\text{N}_2\text{S}$ (2.28 gm) with vigorous stirring carried out for 30 minutes for the formation of a homogenous solution. Afterward, the solution was transferred to an autoclave and heated at 220°C for 24 hours, further cooling it to room temperature. The obtained solution was centrifuged to collect the formed black precipitate. Further, the solution was first washed 3-4 times using DW, followed by 2-3 times with ethanol. In the final stage, the product was dried in a vacuum oven for 24 hours at 60°C [33].

2.2. Synthesis of Pt NPs.

For the synthesis of citrate-capped Pt NPs, a method developed by Henglein and co-workers was adopted. A mixture was prepared of 0.0003 M in 97 mL DW containing $\text{H}_2\text{PtCl}_6 \cdot 6\text{H}_2\text{O}$ (3 mL of 0.01 M). The mixture was then heated with continuous stirring at 100°C . After that 1%, $\text{Na}_3\text{C}_6\text{H}_5\text{O}_7$ was prepared, and 5 mL of it was mixed into the solution. In addition, the yellow color of the solution turned transparent and further to light brown. The

obtained product was allowed to boil for 30 more minutes, and then it was cooled at room temperature to form Pt nanoparticles [35].

2.3. Preparing MIP.

To synthesize MIP for GA, the bulk polymerization method was adopted. All the reagents (EGDMA, MMA, GA) were added in a specific ratio of 1:4:4 M in a porogen (ACN-50 mL). Further, the prepared mixture was allowed to sonicate for about 30 minutes and kept under purging for 10 minutes. Maintaining the inert conditions, the mixture was thermally polymerized with an AIBN initiator at 40 °C for 2 days in a water bath. After 48 hours, a white crystalline powder was obtained. Now, this obtained product was washed using a methanol-acetic acid mixture. In the next step, the MIP was kept for drying in an oven and ground into fine powder for further experimentation [26].

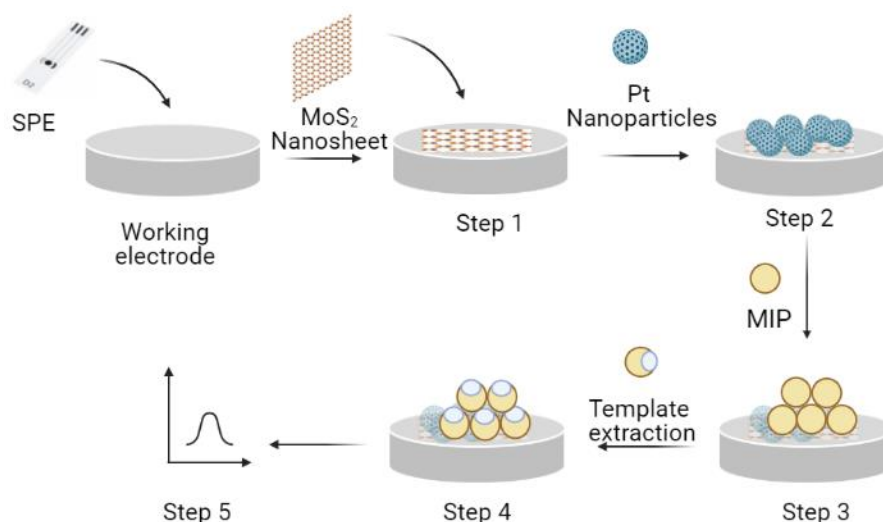
2.4. Fabrication of working screen-printed electrode.

2.4.1. Modifying surface of SPE with MoS₂ nanosheets.

A solution of MoS₂ (0.1 gm) in DW (10 mL) was prepared with 30 minutes of sonication. For the thin and uniform deposition of MoS₂ nanosheets, the cyclic voltammetry (CV) technique was incorporated. A 100 µL of the prepared solution was drop cast on the electrode surface, and CV cycles (10 cycles for polymerization) were applied from 0.0 to -1.0 V at 50 mV/s. Then afterward, DW was used for washing the surface of the electrode to remove unbounded particles and then drying the electrode at room temperature [36].

2.4.2. Electrodepositing Pt NPs on MoS₂/SPE modified electrode.

A 100 µL of synthesized Pt NPs solution (light brown) dropped cast on a modified MoS₂/SPE surface. The Pt NPs were electrodeposited with the CV technique using a voltage from -0.5 to 1.5 V and a scan rate of 50 mV/s for 25 cycles [34,37].



Scheme 1. Stepwise graphical representation for the development of the biosensor: Step 1: Electrodeposition of MoS₂ nanosheet on a screen-printed electrode (SPE); Step 2: Deposition of Pt NPs on modified MoS₂/SPE; Step 3: Electrode modification with molecular imprinted polymer (MIP); Step 4: Extraction of template from the bulk MIP; Step 5: Electrochemical measurement for the modified electrode (SPE-Screen printed electrode; MMA-Methyl methacrylate; EGDMA-Ethylene glycol dimethylacrylate; AIBN-Azobisisobutyronitrile; ACN-Acetonitrile; GA-Glycated Albumin; MIP-Molecular imprinted polymer).

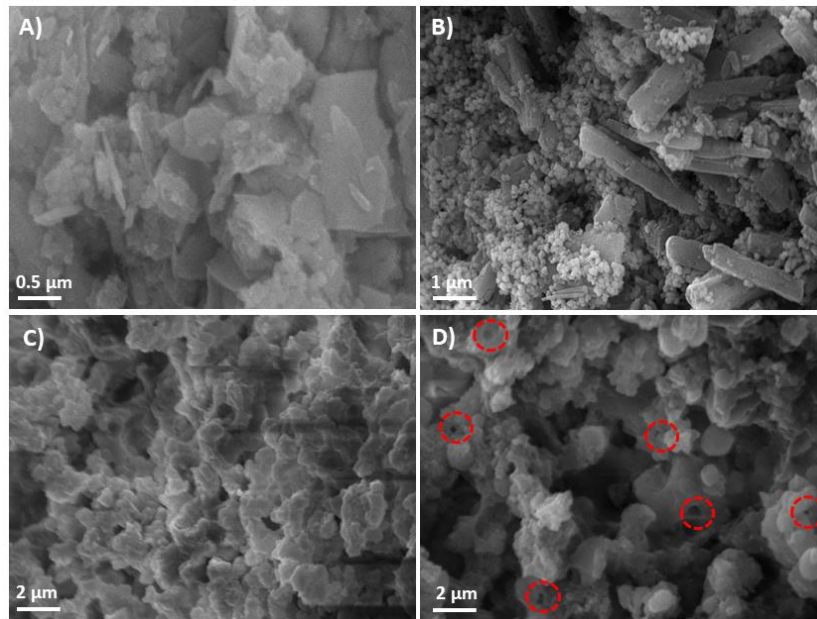
2.4.3. Electrodeposition of MIP on Pt NPs/MoS₂/SPE.

Afterward, the surface of the designed electrode (Pt NPs/MoS₂/SPE) was modified using MIP prepared for GA. The CV technique was used, and voltage was applied from -0.2 to 0.6 V for 15 cycles at a scan rate of 20 mV/s. After the deposition of MIP on the electrode surface, it was washed with DW. Further, the electrode was stored at normal temperature for drying to perform other experiments [26]. The fabrication steps for the electrode are clearly illustrated in Scheme 1. The cavities formed on the electrode surface for the GA molecules allow for rapid and fast transfer of electrons on the surface, resulting in an enhancement of electron conductivity.

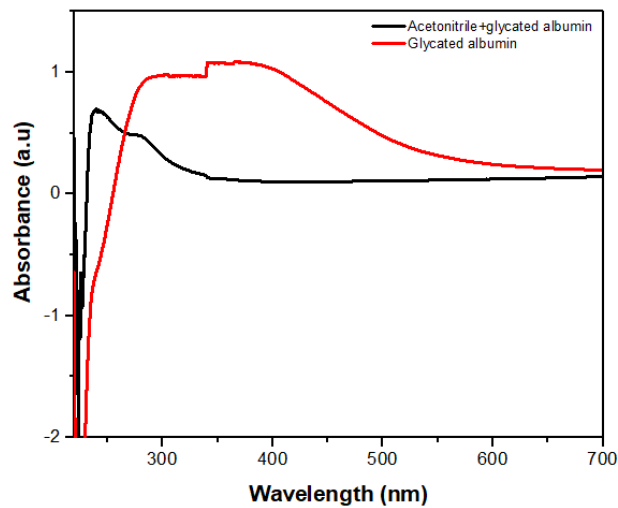
3. Results and Discussion

3.1. Morphology characterization of the designed MIP/Pt NPs/MoS₂/SPE.

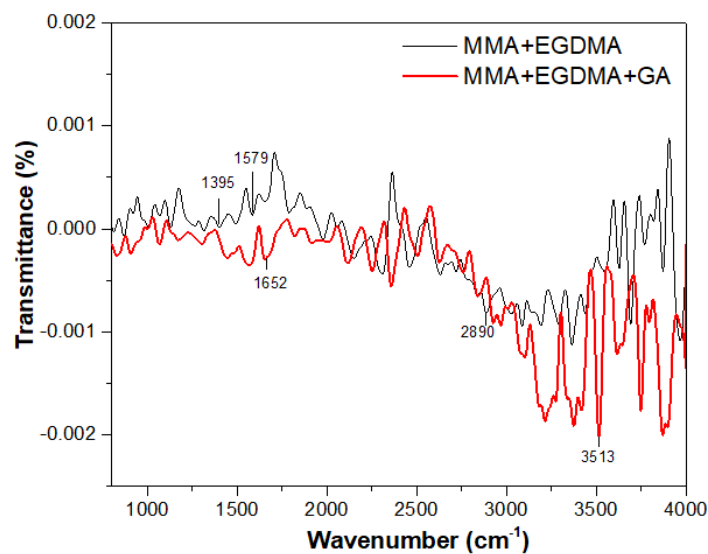
The surface of the designed (MIP/Pt NPs/MoS₂/SPE) electrode was characterized with SEM at each modification stage. Figure 1(i)(A) illustrates the SEM micrograph of MoS₂ nanosheets at 0.5 μm. The image clearly shows the formation of sheet-like structures on the electrode surface for MoS₂ to provide a large surface area. Figure 1(i)(B) represents the Pt NPs on MoS₂/SPE electrode surface. The spherical-like structures confirm the existence of nanoparticles on the surface of Pt NPs/MoS₂/SPE. The Pt NPs provide higher catalytic activity to the biosensor. Figure 1(i)(C) depicts the SEM image for the MIP coated on Pt NPs/MoS₂/SPE electrode surface. It can be seen that similar structures are present on the electrode surface, confirming the deposition of MIP on an electrode. Figure 1(i)(D) describes the SEM for MIP-washed; that is, the template is removed from the bulk polymer. The cavities observed on the surface of the electrode show that the template is extracted from the polymer. To determine the denaturation of GA, the samples (GA and GA+acetonitrile) were characterized with ultra-violet spectroscopy as described in Figure 1(ii). The absorbance peak was obtained within the 200-300 nm range due to the existence of aromatic amino acids in both cases. Therefore, it can be concluded that no denaturation problem occurred. The functional groups of the samples (MMA+EGDMA and MMA+EGDMA+GA) were determined with Fourier Transform Infrared (FTIR) Spectroscopy illustrated in Figure 1(iii). The peaks at 2890 cm⁻¹ and 159 cm⁻¹ confirm the presence of C-H and -C=C stretching vibrations, respectively. The various peaks obtained in the range from 1250-11000 cm⁻¹ show C-O stretching in C-O-CH₃. The peaks obtained from 886-800 cm⁻¹ represent 1,4-substituted aromatic rings. In the case of GA, peaks ranging from 1800-1700 cm⁻¹ show C=O stretching vibration of lipid. The range from 1685-1630 cm⁻¹ shows amide carbonyl. The band from 1640-1600 cm⁻¹ represents NH₂ angle-variable vibration in R-CONH₂. The peak at 3513 cm⁻¹ indicates the O-H group in GA, stating the hydrophilic nature [38,39]. The binding of the template and MIP was due to the noncovalent interaction (hydrophobic effects, ionic interaction, hydrogen bonding, van der Waals forces, π-π interactions) [40].



(i)



(ii)



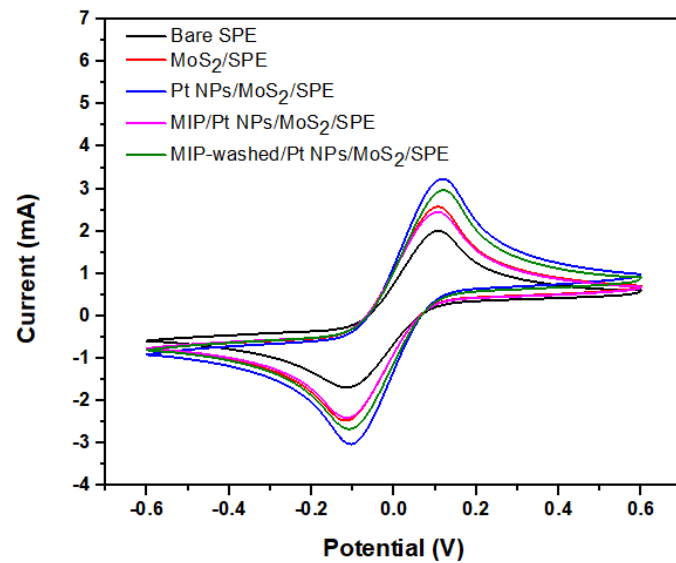
(iii)

Figure 1. (i) Scanning electron microscopy: Surface study of modified electrode with scanning electron microscopy: (A) MoS₂/SPE, (B) Pt NPs/MoS₂/SPE, (C) MIP/Pt NPs/MoS₂/SPE, and (D) MIP-washed/Pt NPs/MoS₂/SPE; (ii) Ultraviolet-visible spectroscopy for GA and acetonitrile+GA; (iii) Fourier Transform Infrared (FTIR) Spectroscopy for GA and MMA+EGDMA+GA.

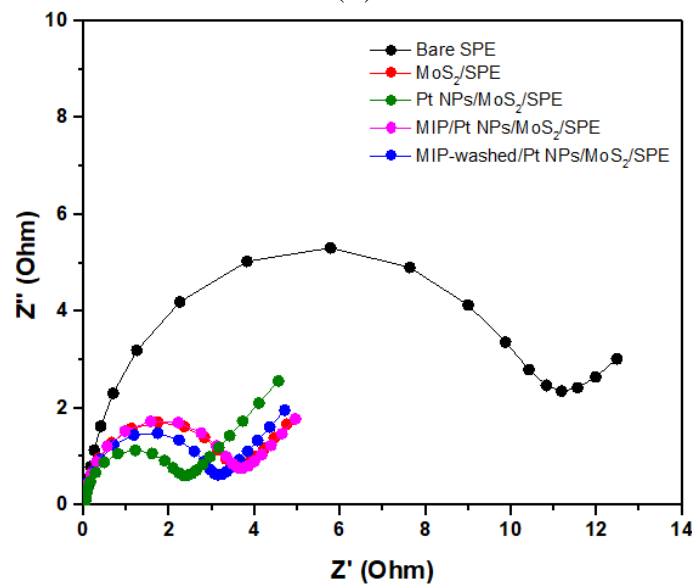
3.2. Electrochemical measurement for stepwise modification of fabricated MIP-washed/Pt NPs/MoS₂/SPE.

3.2.1. Cyclic voltammetry studies.

The designed MIP-washed/Pt NPs/MoS₂/SPE electrode was evaluated with CV measurements, as shown in Figure 2(A). The difference in oxidation and reduction peaks shows the modification that occurred on the surface of the electrode. The bare electrode shows the lowest oxidation and reduction peaks at +2 mA and -1.7 mA, respectively when observed in ferrocyanide/ferricyanide electrolyte solution of 5 mM. When the SPE was modified with MoS₂ the oxidation (I_{pa}) and reduction (I_{pc}) peaks increased to +2.5 mA and -2.4 mA, respectively.



(A)



(B)

Figure 2. Electrode modification: Response of developed biosensor with CV and electrochemical impedance spectroscopy (EIS) measurements (A) CV curve for stepwise modification stages of the electrode Bare SPE, MoS₂/SPE, Pt NPs/MoS₂/SPE, MIP/Pt NPs/MoS₂/SPE, and MIP-washed/PtNPs/MoS₂/SPE within a potential range from -0.6 to 0.6 V in a ferrocyanide/ferricyanide electrolyte solution of 5 mM; (B) EIS for different stages of modified electrode Bare SPE, MoS₂/SPE, PtNPs/MoS₂/SPE, MIP/PtNPs/MoS₂/SPE, MIP-washed/Pt NPs/MoS₂/SPE the EIS studies were carried at frequency F_{initial}-100 KHz to F_{final}-100 mHz.

The presence of MoS₂ nanosheets on the electrode surface leads to an enhancement in the surface area. This results in higher electron transfer in the presence of an electron mediator on the electrode surface. Hence, the peak currents for oxidation and reduction curves were enhanced. With further modification using Pt NPs, oxidation and reduction peaks were enhanced. The Pt NPs act as an electrochemical catalyst that facilitates accelerating the rate of reaction occurring on the electrode surface. Also, Pt NPs enhance the electron transfer on the modified electrode surface, leading to higher electrode conductivity. When the MIP was integrated on the surface of the designed SPE, the I_{pa} and I_{pc} peaks decreased. The MIP is a polymer whose presence on the surface results in a decrement of the current flow. But the current increased when the template was removed from the bulk MIP. This enhancement in current was observed due to the cavities that are formed on the electrode surface. After template removal, more electroactive sites were generated, and enhancement in electron flow was observed.

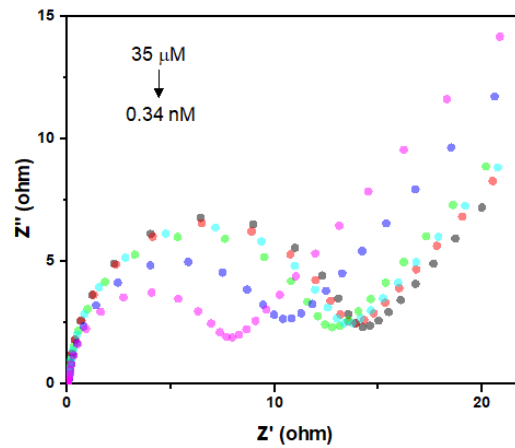
3.2.2. Impedance studies.

Impedance studies were done to observe the electrode surface's resistance with each modification stage. The electrochemical impedance spectroscopy (EIS) curve can be obtained using the Nyquist plot and the Bode plot. Figure 2(B) illustrates each stage's Nyquist plot for the modified electrodes. It is represented in two parts, a semi-circle, and a linear graph. The semi-circle part of the Nyquist provides information about the resistance charge transfer (R_{ct}) value, and the linear part of the graph gives the diffusion process. Figure 2(B) clearly shows that in the modification stages, the R_{ct} value changes. A higher R_{ct} curve was obtained with the bare electrode (11.19Ω); when the electrode was modified with MoS₂, the R_{ct} value decreased to 3.334Ω due to the higher electron generation on the surface of the electrode. In the next step, the electrode was modified with Pt NPs to provide the catalytic activity of the biosensor. The R_{ct} observed was 2.34 Ω. The electrode was modified with MIP for GA, and the R_{ct} value obtained was 3.77 Ω. Further, when the electrode was washed to remove the molecules of GA from the electrode surface and obtain its imprints, a decrement in the R_{ct} value to 3.09 Ω was observed.

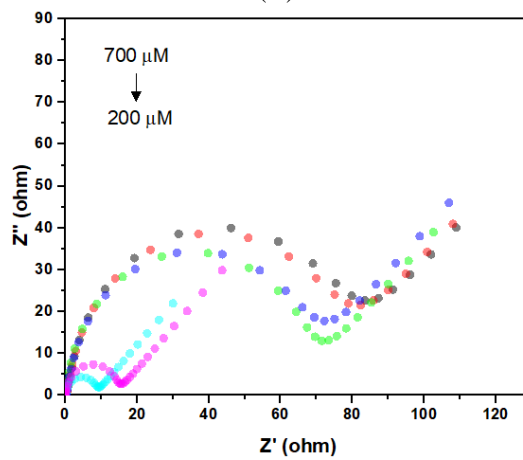
3.3. Different concentration study on modified electrode (MIP-washed/Pt NPs/MoS₂/SPE).

The designed biosensor executes a dynamic concentration range from 0.34 nM to 700 μM. For clear understanding, the concentration range was divided into two: lower (0.34 nM to 35 μM) and higher (200 to 700 μM) ranges in a ferrocyanide/ferricyanide electrolyte solution (5 mM). Figure 3(A) and 3(B) show the EIS graphs for the developed biosensor with lower and higher concentration ranges from 0.34 nM to 35 μM and 200 to 700 μM, respectively. Figure 3(C) and 3(D) demonstrate the calibration curve for varying concentration versus R_{ct} value for both cases (lower and higher concentration range). It was observed that the resistance on the electrode decreased with the decrease in concentration. This condition was observed because the increasing concentrations of GA on the electrode surface block the molecules from binding to the MIP. Therefore, large resistance is created on the surface, whereas at lower concentrations, low resistance is generated [41]. Figure 3(E) and (F) illustrate the square wave voltammetry (SWV) response of the biosensor with a varying concentration in a lower and higher range. The study provides information about the change in current flow with the changing concentration; high concentration resulted in a lower current generation. The

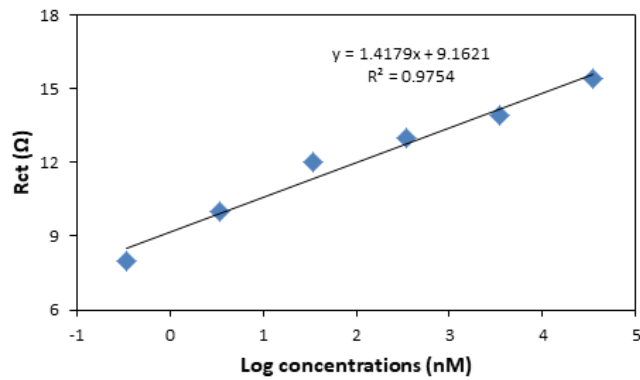
biosensor shows a 0.34 nM concentration as a lower detection limit. The sensitivity of the biosensor was calculated as 0.40 Ω /nM.



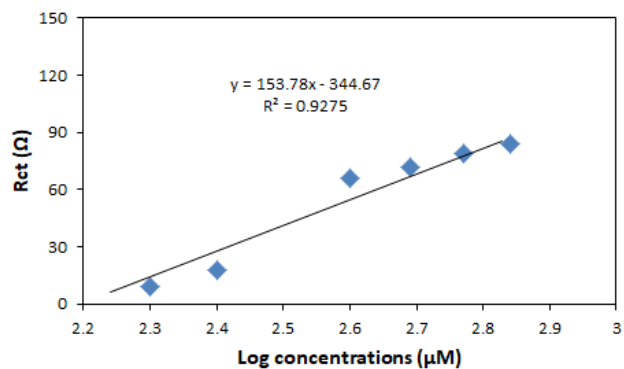
(A)



(B)



(C)



(D)

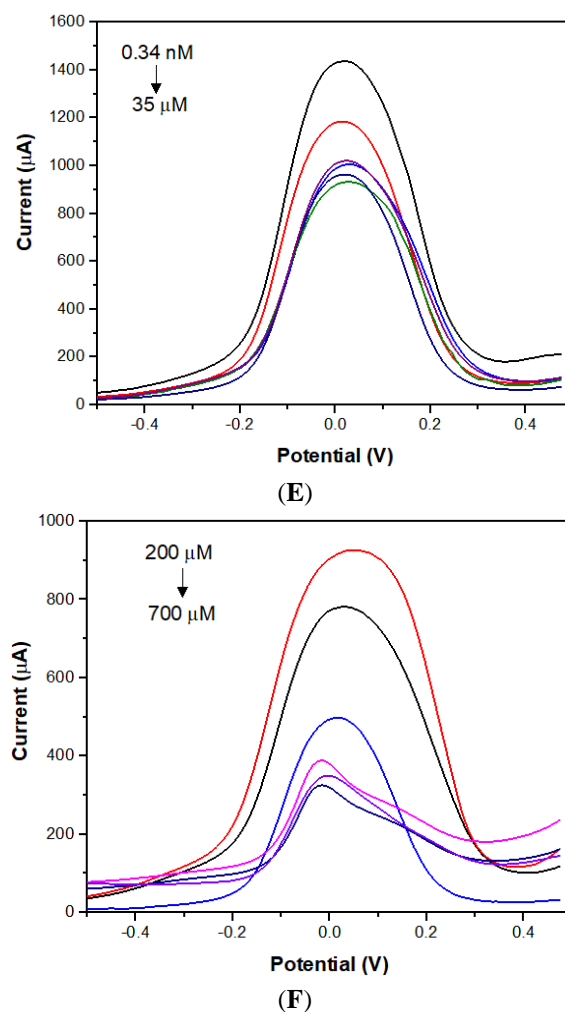
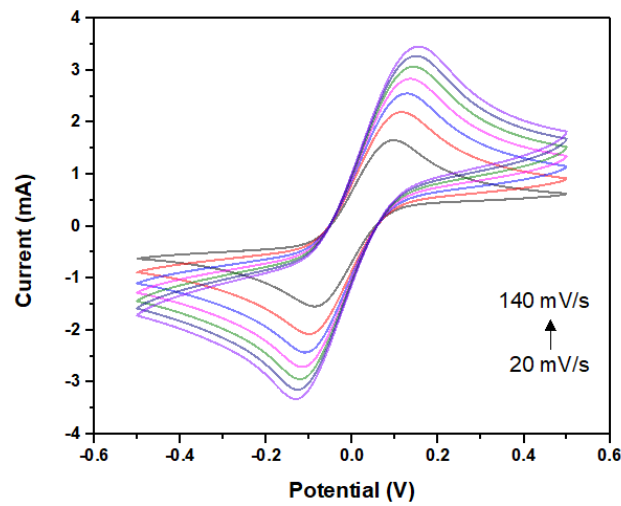


Figure 3. Varying concentrations on electrode surface: Electrochemical impedance spectroscopy (EIS) curve for the concentrations of GA (A) 0.34 nM to 35 μM (lower concentration range); (B) 200 to 700 μM (higher concentration range) on the modified electrode at frequency $F_{initial}$ -100 KHz to F_{final} -100 mHz. Calibration graph of EIS response obtained with varying concentrations of GA; (C) 0.34 nM to 35 μM (lower concentration range); (D) 200 to 700 μM (higher concentration range). Square wave voltammetry measurements for different concentrations of GA; (E) 0.34 nM to 35 μM (lower concentration range); (F) 200 to 700 μM (higher concentration range).

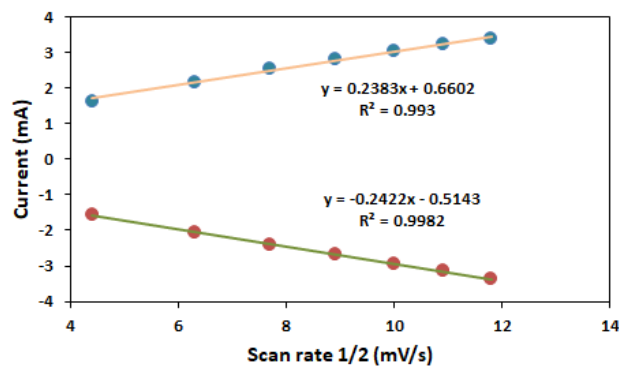
3.4 Optimizing parameters for MIP-washed/Pt NPs/MoS₂/SPE.

3.4.1. Scan rate studies for MIP-washed/Pt NPs/MoS₂/SPE.

The scan rate studies can give a clear view of the steady electron-transfer kinetics for the designed *MIP-washed/Pt NPs/MoS₂/SPE*. Therefore, for examining this scan rate, studies were performed from 20 to 140 mV/s in a ferrocyanide/ferricyanide electrolyte solution, and a voltage range of -0.5 to 0.5 V. Figure 4(A) describes the scan rate graph with different values from 20 to 140 mV/s with a difference of 20 mV/s. It was observed that with the increasing scan rate, the I_{pa} and I_{pc} increased gradually. Figure 4(B) illustrates the linear calibration curve that is plotted between the square root value function of scan rate (\sqrt{v}) versus I_{pa} and I_{pc} (Table S1) for each scan rate. The plotted graph describes that a linear increase is obtained with the I_{pa} and I_{pc} with the enhanced scan rate values.



(A)

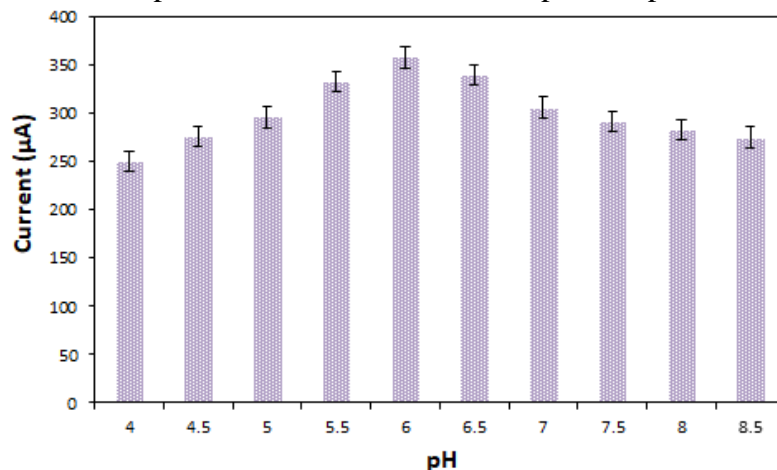


(B)

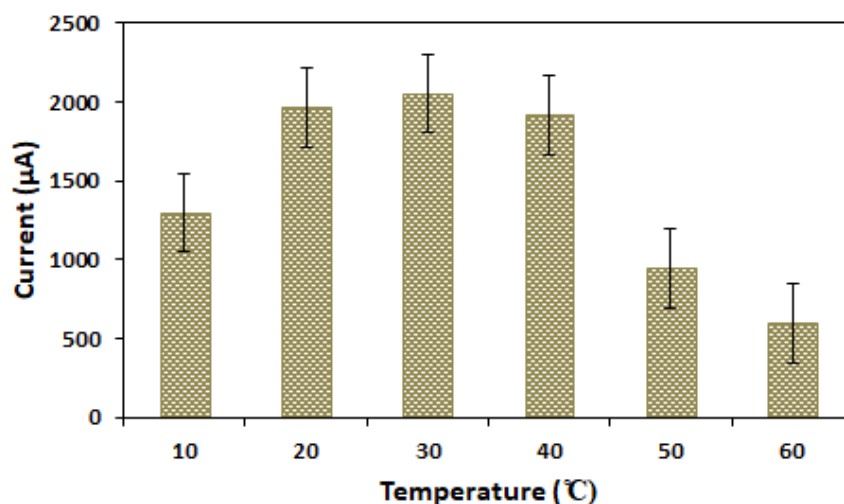
Figure 4. Scan rate studies: (A) Scan rate study for the developed biosensor from 20 mV/s to 140 mV/s; (B) Graph for the square root of scan rate vs. oxidation and reduction peaks.

3.4.2. Effect of pH and temperature on the developed biosensor.

The optimum pH of the biosensor was evaluated with pH solutions for distinct pH values from 4 to 8.5, as shown in Figure 5(A). The plotted bar graph describes the peak current obtained from the square wave voltammetry (SWV) studies that were accomplished in a ferrocyanide/ferricyanide electrolyte solution (5 mM) at potential -0.5 V. It was observed that the peak current increased from 4 to 6 pH. Whereas a gradual decrease was obtained in the peak current beyond 6 pH because of the formation of hydrogen bonds on the surface of the electrode [42]. Therefore, 6 pH was determined to be the optimum pH for further experiments.



(A)



(B)

Figure 5. Optimized pH and temperature: (A) pH studies for the assembled electrode ranging from 4 to 8.5 with an interval of 0.5 units. The study was obtained in an electrolyte (ferrocyanide/ferricyanide) of 5 mM at -0.5 V; (B) Temperature graph for modified electrode ranging from 10 °C to 60 °C with each interval of 10 °C.

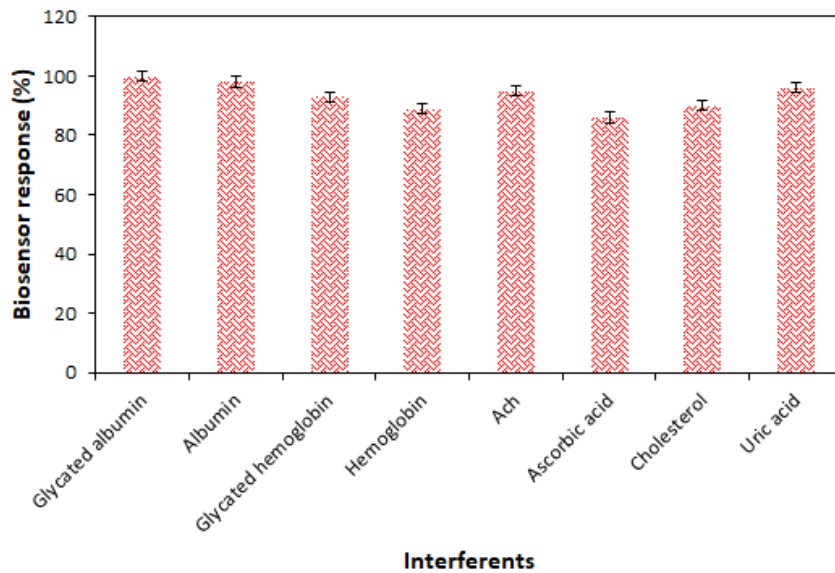
3.4.3. Temperature effect on fabricated MIP-washed/Pt NPs/MoS₂/SPE electrode

The effect of temperature was observed on the *MIP-washed/Pt NPs/MoS₂/SPE electrode* from 10 to 60 °C with a difference of 10 °C in a ferrocyanide/ferricyanide electrolyte solution (5 mM) using SWV measurements at -0.5 V. Figure 5(B) illustrate results from SWV studies that were carried out with distinct temperature value. The graphs show that a higher current value was obtained at a temperature of 30 °C. After 30 °C the current value was decreased; the decline in peak current value can be occurred due to the molecule interaction between functional monomers and template. The highest current generation at 30 °C made it to be considered the optimum temperature for the designed sensing platform.

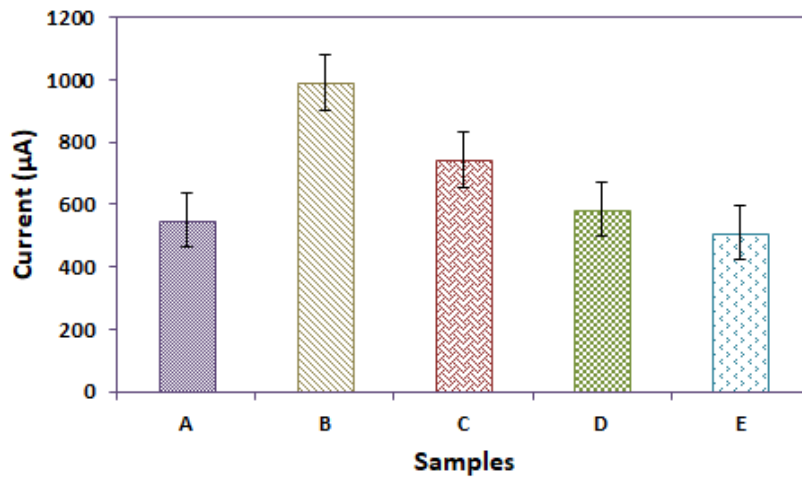
3.5. Interference, clinical validation, repeatability, and stability of the developed MIP-washed/Pt NPs/MoS₂/SPE biosensor.

3.5.1. Effect of interference on the developed MIP-washed/Pt NPs/MoS₂/SPE electrode

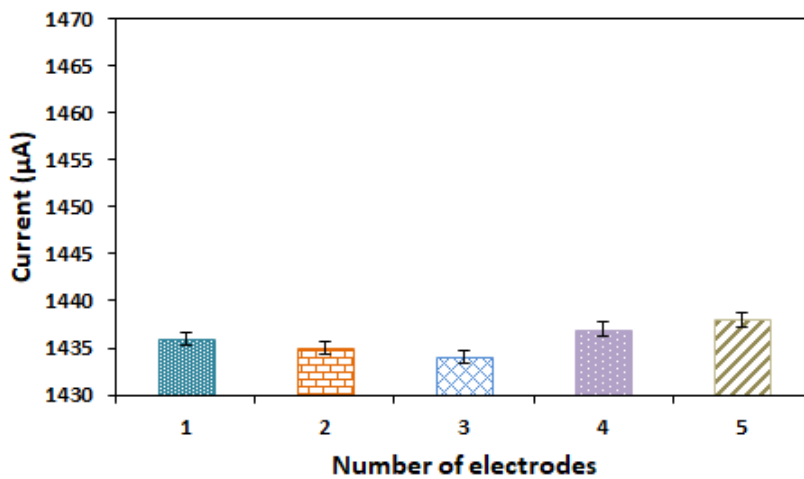
To study interference on the electrode surface, the biosensor was evaluated with different compounds such as GA, -glycated hemoglobin, hemoglobin, cholesterol (C₂₇H₄₆O), acetylcholine (Ach), uric acid (C₅H₄N₄O₃), ascorbic acid (C₆H₈O₆) in a ferrocyanide/ferricyanide electrolyte (5 mM) with GA concentration of 0.34 nM. Figure 6(A) describes the graph for biosensor activity loss (%) with different interference compounds. The loss in biosensor activity was calculated as 2% (albumin), 7% (glycated hemoglobin), 11% (hemoglobin), 5% (Ach), 14% (ascorbic acid), 10% (cholesterol), 4% (uric acid).



(A)



(B)



(C)

Figure 6. Evaluation of developed biosensor: (A) Interference studies on the fabricated biosensor with different interferents (GA, albumin, Glycated hemoglobin, hemoglobin, Acetylcholine (Ach), Ascorbic acid, cholesterol, and Uric acid) with a concentration of 0.34 nM in a ferrocyanide/ferricyanide electrolyte solution (5 mM); (B) Current value obtained with real samples on the developed biosensor; (C) Reproducibility of the electrode when with similar conditions.

3.5.2. Clinical spiked sample validation on the MIP-washed/Pt NPs/MoS₂/SPE electrode.

The fabricated SPE was evaluated with various clinical samples, as represented in Figure 6(B). The graph presents the peak current values obtained during SWV studies with different spiked samples A (3.5 μM), B (0.34 nM), C (3.49 nM), D (350 nM), and E (35 μM). Random unknown samples were taken for electrode evaluation. The higher current was observed, with sample B showing a lower concentration of GA in the sample. On the other hand, sample E shows the lowest current and describes a higher concentration of the GA in the sample.

3.5.3. Repeatability and stability of the developed biosensor

To evaluate the repeatability of data for the biosensor, five identical types of electrodes were prepared. All the electrodes were prepared and evaluated under similar conditions. Figure 6(C) describes the bar graph for the five electrodes used to study the electrode data's repeatability. It was observed that the current difference between these electrodes was minimum. Hence it can be concluded that the system shows good repeatability.

The electrode stability was examined for 3 months. The designed electrode was stored at 4°C and maintained dry conditions. The electrode was evaluated every 7th day. It was observed that after 3 months, the activity of the electrode decreased from 100% to 80%. Further, after 5 months, it was examined that the activity of the biosensor was reduced to 50%. Table 1 gives a comparison between the fabricated biosensor and reported sensors. It was observed that the biosensor could function in a broad concentration range and exhibit a lower detection limit. The response time of the developed biosensor was obtained as 5 minutes.

Table 1. Comparison of the fabricated and reported biosensor.

S.No.	Detector molecule	Sensing platform	Biosensor type	Detection range	Detection limit	Response time	Regression coefficient	Ref.
1.	Aptamer	GC/rGO-AuNPs/Apt-GA	Electrochemical	2-10 μg/mL	0.07 μg/mL	NR*	NR	[22]
2.	Enzyme	Ab-uPtNZ/GA/BA-agarose bead complex	Electrochemical	5000-100000 μg/mL	3.8 μg/mL	20 min.	0.98	[24]
3.	Enzyme	Ab-uPtNZ/GA/BA-agarose bead complex	Colorimetric	10 μg/mL-5000 μg/mL	9.2 μg/mL	20 min.	0.97	[24]
4.	Aptamer	GHSA-specific aptamers	Fluorescence	3400-31300 μg/mL	50 μg/mL	30 min.	0.98	[25]
5.	Enzyme	Interdigitated electrodes	Electrochemical	0-33350 μg/mL	80.04 μg/mL	1 min	0.99	[10]
6.	Enzyme	APBA-modified PBNPs	Colorimetric	10000-2000 μg/mL	7320 mg/mL	10 min.	0.99	[43]
7.	Enzyme	APBA-modified PBNPs	Electrochemical	5000-1000 μg/mL	3470 μg/mL	10 min.	0.99	[43]
8.	MIP	MIP-washed/Pt NPs/MoS ₂ /SPE	Electrochemical	0.02267 μg/mL-46690 μg/mL	0.02267 μg/mL	< 3 min.	0.98	Present work

4. Conclusions

In this present study, a biosensing platform based on electrochemical detection was developed for detecting the concentration of GA. GA provides highly accurate results for the concentration change in plasma and postprandial plasma glucose within the short term rather

than other protein markers. Also, it provides glycemic control for patients suffering from hematologic disorders. Therefore, this designed biosensor can facilitate the advance and fast determination of GA levels in a sample. Furthermore, the developed device can be miniaturized, portable, and easily handled. The developed platform is based on the molecular imprinting technique that provides higher specificity to the biosensor and requires low-cost development. Further, integrating nanomaterials on the electrode surface provides higher conductivity and a large surface area. Hence, this fabricated platform can help develop a future medical application for the early diagnosis of diabetes.

Funding

This research received external funding from Biotechnology Industry Research Assistance Council (BIRAC) (File No. BT/IIPME0211/02/16).

Conflicts of Interest

The authors declare no competing interest in this presented manuscript.

References

1. Guber, K.; Pemmasani, G.; Malik, A.; Aronow, W.S.; Yandrapalli, S.; Frishman, W.H. Statins and higher diabetes mellitus risk: incidence, proposed mechanisms, and clinical implications. *Cardiology in Review* **2021**, *29*, 314-2. <https://doi.org/10.1097/CRD.0000000000000348>.
2. Yandrapalli, S.; Jolly, G.; Horblitt, A.; Pemmasani, G.; Sanaani, A.; Aronow, W.S.; Frishman, W.H. Cardiovascular Safety and Benefits of Noninsulin Antihyperglycemic Drugs for the Treatment of Type 2 Diabetes Mellitus—Part 1. *Cardiology in review* **2020**, *28*, 177-189, <https://doi.org/10.1097/CRD.0000000000000311>.
3. Belsare, S.; Coté, G. Development of a colorimetric paper fluidic dipstick assay for measurement of glycated albumin to monitor gestational diabetes at the point-of-care. *Talanta* **2021**, *223*, 121728, <https://doi.org/10.1016/j.talanta.2020.121728>.
4. Matoori, S.; Veves, A.; Mooney, D.J. Advanced bandages for diabetic wound healing. *Science Translational Medicine* **2021**, *13*, eabe4839, <https://doi.org/10.1126/scitranslmed.abe4839>.
5. Waiwinya, W.; Putnin, T.; Pimalai, D.; Chawjiraphan, W.; Sathirapongsasuti, N.; Japrun, D. Immobilization-Free Electrochemical Sensor Coupled with a Graphene-Oxide-Based Aptasensor for Glycated Albumin Detection. *Biosensors* **2021**, *11*, 85, <https://doi.org/10.3390/bios11030085>.
6. Zendjabil, M. September. Glycated hemoglobin: indication, interpretation and limits. In *Annales Pharmaceutiques Françaises, Elsevier Masson* **2015**, *73*, 336-339, <https://doi.org/10.1016/j.pharma.2015.03.001>.
7. Rohlfing, C.L.; Wiedmeyer, H.M.; Little, R.R.; England, J.D.; Tennill, A.; Goldstein, D.E. Defining the relationship between plasma glucose and HbA1c: analysis of glucose profiles and HbA1c in the Diabetes Control and Complications Trial. *Diabetes care* **2002**, *25*, 275-278, <https://doi.org/10.2337/diacare.25.2.275>.
8. Zendjabil, M. Biological diagnosis of diabetes mellitus. *Current Research in Translational Medicine* **2016**, *64*, 49-52, <https://doi.org/10.1016/j.patbio.2015.10.002>.
9. Ferrario, L.; Schettini, F.; Avogaro, A.; Bellia, C.; Bertuzzi, F.; Bonetti, G.; Ceriello, A.; Ciaccio, M.; Romanelli, M.C.; Dozio, E.; Falqui, L. Glycated albumin for glycemic control in T2DM population: a multi-dimensional evaluation. *ClinicoEconomics and Outcomes Research: CEOR* **2021**, *13*, 453, <https://doi.org/10.3390/molecules26030734>.
10. Hatada, M.; Loew, N.; Okuda-Shimazaki, J.; Khanwalker, M.; Tsugawa, W.; Mulchandani, A.; Sode, K. Development of an Interdigitated Electrode-Based Disposable Enzyme Sensor Strip for Glycated Albumin Measurement. *Molecules* **2021**, *26*, 734, <https://doi.org/10.3390/molecules26030734>.
11. Valenzano, M.; Bertolotti, I.C.; Valenzano, A.; Grassi, G. Time in range—A1c hemoglobin relationship in continuous glucose monitoring of type 1 diabetes: a real-world study. *BMJ Open Diabetes Research and Care* **2021**, *9*, e001045, <https://doi.org/10.1136/bmjdr-2019-001045>.

12. Perejda, A.J. Vascular and cutaneous complications of diabetes mellitus: The role of nonenzymatic glycosylation of collagens. *InConnective Tissue Disease* **2021**, 475-490, <https://doi.org/10.1201/9781003210016>.
13. Zendjabil, M. Glycated albumin. *Clinica Chimica Acta* **2020**, 502, 240-244, <https://doi.org/10.1016/j.cca.2019.11.007>
14. Testa, R.; Ceriotti, F.; Guerra, E.; Bonfigli, A.R.; Boemi, M.; Cucchi, M.; Di Gaetano, N.; Santini, G.; Genovese, Ceriello, A. Glycated albumin: correlation to HbA1c and preliminary reference interval evaluation. *Clinical Chemistry and Laboratory Medicine (CCLM)* **2017**, 55, e31-33, <https://doi.org/10.1515/cclm-2016-0512>.
15. Ciaccio, M. Introduction of glycated albumin in clinical practice. *J. Lab. Precis. Med.* **2019**, 4, 28, <https://doi.org/10.21037/jlpm.2019.08.02>.
16. Kohzuma, T.; Tao, X.; Koga, M. Glycated albumin as biomarker: evidence and its outcomes. *Journal of Diabetes and its Complications* **2021**, 35, 108040, <https://doi.org/10.1016/j.jdiacomp.2021.108040>.
17. Dong, Y.; Zhai, Y.; Wang, J.; Chen, Y.; Xie, X.; Zhang, C.; Liu, J.; Lu, Y.; Tang, G.; Han, L.; Li, L. Glycated albumin in pregnancy: reference intervals establishment and its predictive value in adverse pregnancy outcomes. *BMC Pregnancy and Childbirth* **2020**, 20, 1-9, <https://doi.org/10.1186/s12884-019-2704-x>.
18. Robinson, T.W.; Freedman, B.I. Glycated albumin and blood sugar control in advanced chronic kidney disease. *Nephrology Dialysis Transplantation* **2018**, 33, 1087-90, <https://doi.org/10.1093/ndt/gfy059>.
19. Rondeau, P.; Bourdon, E. The glycation of albumin: structural and functional impacts. *Biochimie* **2011**, 93, 645-58, <https://doi.org/10.1016/j.biochi.2010.12.003>.
20. Koga, M.; Kasayama, S. Clinical impact of glycated albumin as another glycemic control marker. *57*, 751-762. *Endocrine journal* **2010**, , <https://doi.org/10.1507/endocrj.K10E-138>.
21. Cheeveewattanagul, N.; Yévenes, C.F.; Bamrungsap, S.; Japrun, D.; Chalermwatanachai, T.; Siriwan, C.; Warachit, O.; Somasundrum, M.; Surareungchai, W.; Rijiravanich, P. Aptamer-functionalised magnetic particles for highly selective detection of urinary albumin in clinical samples of diabetic nephropathy and other kidney tract disease. *Analytica Chimica Acta* **2021**, 1154:338302, <https://doi.org/10.1016/j.aca.2021.338302>.
22. Farzadfard, A.; Shayeh, J.S.; Habibi-Rezaei, M.; Omid, M. Modification of reduced graphene/Au-aptamer to develop an electrochemical based aptasensor for measurement of glycated albumin. *Talanta* **2020**, 211, 120722, <https://doi.org/10.1016/j.talanta.2020.120722>.
23. Freitas, P.A.; Ehlert, L.R.; Camargo, J.L. Glycated albumin: a potential biomarker in diabetes. *Archives of endocrinology and metabolism* **2017**, 61, 296-304, <https://doi.org/10.1590/2359-3997000000272>.
24. Choi, H.; Son, S.E.; Hur, W.; Tran, V.K.; Lee, H.B.; Park, Y.; Seong, G.H. Electrochemical immunoassay for Determination of Glycated Albumin using nanozymes. *Scientific reports* **2020**, 10, 1-12, <https://doi.org/10.1038/s41598-020-66446-3>.
25. Apiwat, C.; Luksirikul, P.; Kankla, P.; Pongprayoon, P.; Treerattrakoon, K.; Paiboonsukwong, K.; Fucharoen, S.; Dharakul, T.; Japrun, D. Graphene based aptasensor for glycated albumin in diabetes mellitus diagnosis and monitoring. *Biosensors and Bioelectronics* **2016**, 82, 140-145, <https://doi.org/10.1016/j.bios.2016.04.015>.
26. Jain, U.; Soni, S.; Balhara, Y.P.S.; Khanuja, M.; Chauhan, N. Dual-Layered Nanomaterial-Based Molecular Patterning on Polymer Surface Biomimetic Impedimetric Sensing of a Bliss Molecule, Anandamide Neurotransmitter. *ACS omega* **2020**, 5, 10750-10758, <https://doi.org/10.1021/acsomega.0c00285>.
27. Balayan, S.; Chauhan, N.; Chandra, R.; Jain, U. Electrochemical Based C-Reactive Protein (CRP) Sensing Through Molecularly Imprinted Polymer (MIP) Pore Structure Coupled with Bi-Metallic Tuned Screen-Printed Electrode. *Biointerface Res. Appl. Chem.* **2022**, 6, 38, <https://doi.org/10.33263/BRIAC126.76977714>.
28. Balayan, S.; Chauhan, N.; Kumar, P.; Chandra, R.; Jain, U. Fabrication of a sensing platform for identification of tumor necrosis factor-alpha: a biomarker for neonatal sepsis. *3 Biotech* **2022**, 12, 1-3, <https://doi.org/10.1007/s13205-021-03083-1>.
29. Balayan, S.; Chauhan, N.; Chandra, R.; Jain, U. Molecular imprinting based electrochemical biosensor for identification of serum amyloid A (SAA), a neonatal sepsis biomarker. *International Journal of Biological Macromolecules* **2022**, 195, <https://doi.org/10.1016/j.ijbiomac.2021.12.045>.
30. Rohaizad, N.; Mayorga-Martinez, C.C.; Fojtů, M.; Latiff, N.M.; Pumera, M. Two-dimensional materials in biomedical, biosensing and sensing applications. *Chemical Society Reviews* **2021**, 50, 619-57, <https://doi.org/10.1039/D0CS00150C>.

31. Jun, S.E.; Hong, S.P.; Choi, S.; Kim, C.; Ji, S.G.; Park, I.J.; Lee, S.A.; Yang, J.W.; Lee, T.H.; Sohn, W.; Kim, J.Y. Boosting Unassisted Alkaline Solar Water Splitting Using Silicon Photocathode with TiO₂ Nanorods Decorated by Edge-Rich MoS₂ Nanoplates. *Small* **2021**, *17*, 2103457, <https://doi.org/10.1002/smll.202103457>.
32. Schmidt, A.; Ramos, M.K.; Ferreira, C.M.; Braz, B.A.; Zarbin, A.J. Molybdenum-based materials/carbon nanotubes nanocomposites prepared as thin and transparent films for aqueous K-ion batteries. *Electrochimica Acta* **2021**, *387*, 138500, <https://doi.org/10.1016/j.electacta.2021.138500>.
33. Hamami, M.; Raouafi, N.; Korri-Youssoufi, H. Self-assembled MoS₂/SsDNA nanostructures for the capacitive aptasensing of acetamiprid insecticide. *Applied Sciences* **2021**, *11*, 1382, <https://doi.org/10.3390/app11041382>.
34. Gupta, S.; Tiwari, A.; Jain, U.; Chauhan, N. Synergistic effect of 2D material coated Pt nanoparticles with PEDOT polymer on electrode surface interface for a sensitive label free Helicobacter pylori CagA (Ag-Ab) immunosensing. *Materials Science and Engineering: C* **2019**, *103*, 109733, <https://doi.org/10.1016/j.msec.2019.05.018>.
35. Jawad, M.; Ali, S.; Waseem, A.; Rabbani, F.; Amin, B.A.Z.; Bilal, M.; Shaikh, A.J. Plasmonic effects and size relation of gold-platinum alloy nanoparticles. *Advances in nano research* **2019**, *7*, 169, <https://doi.org/10.12989/anr.2019.7.3.169>.
36. Jain, U.; Khanuja, M.; Gupta, S.; Harikumar, A.; Chauhan, N. Pd nanoparticles and molybdenum disulfide (MoS₂) integrated sensing platform for the detection of neuromodulator. *Process Biochemistry* **2019**, *81*, 48-56, <https://doi.org/10.1016/j.procbio.2019.03.019>.
37. Kheirmand, M.; Eshghi, A. Electrodeposition of platinum nanoparticles on reduced graphene oxide as an efficient catalyst for oxygen reduction reaction. *Iranian Journal of Hydrogen & Fuel Cell* **2015**, *2*, 7-12, <https://doi.org/10.22104/IJHFC.2015.168>.
38. Wnuczek, K.; Puszka, A.; Klapiszewski, Ł.; Podkościelna, B. Preparation, Thermal, and Thermo-Mechanical Characterization of Polymeric Blends Based on Di (meth) acrylate Monomers. *Polymers* **2021**, *13*, 878, <https://doi.org/10.3390/polym13060878>.
39. Li, Y.; Li, F.; Yang, X.; Guo, L.; Huang, F.; Chen, Z.; Chen, X.; Zheng, S. Quantitative analysis of glycosylated albumin in serum based on ATR-FTIR spectrum combined with SiPLS and SVM. *Spectrochimica Acta Part A: Molecular and Biomolecular Spectroscopy* **2018**, *201*, 249-57, <https://doi.org/10.1016/j.saa.2018.05.022>.
40. Peeters, M.; Eersels, K.; Junkers, T.; Wagner, P. Molecularly imprinted polymers: synthetic receptors for diagnostic medical devices. In *Molecularly Imprinted Catalysts* **2016**, 253-271, <https://doi.org/10.1016/B978-0-12-801301-4.00013-X>.
41. Nguy, T.P.; Van Phi, T.; Tram, D.T.; Eersels, K.; Wagner, P.; Lien, T.T. Development of an impedimetric sensor for the label-free detection of the amino acid sarcosine with molecularly imprinted polymer receptors. *Sensors and Actuators B: Chemical* **2017**, *246*, 461-470, <https://doi.org/10.1016/j.snb.2017.02.101>.
42. Aylaz, G.; Andaç, M.; Denizli, A.; Duman, M. Recognition of human hemoglobin with macromolecularly imprinted polymeric nanoparticles using noncovalent interactions. *Journal of Molecular Recognition* **2021**, *34*, e2935, <https://doi.org/10.1002/jmr.2935>.
43. Son, S.E.; Gupta, P.K.; Hur, W.; Choi, H.; Lee, H.B.; Park, Y.; Seong, G.H. Determination of glycosylated albumin using a Prussian blue nanozyme-based boronate affinity sandwich assay. *Analytica Chimica Acta* **2020**, *1134*, 41-49, <https://doi.org/10.1016/j.aca.2020.08.015>.

Supplementary file

Table S1. Oxidation and reduction peaks for different scan rates.

S.No.	Scan rate (mV/s)	Oxidation peak (mA)	Reduction peak (mA)
1.	20	1.64	-1.54
2.	40	2.18	-2.06
3.	60	2.55	-2.42
4.	80	2.83	-2.68
5.	100	3.07	-2.93
6.	120	3.25	-3.15
7.	140	3.4	-3.35